THE JOURNAL OF PHYSICAL CHEMISTRY C
A JOURNAL OF THE AMERICAN CHEMICAL SOCIETY

pubs.acs.org/JPCC

Article

Effect of Oxygen Poisoning on the Bidirectional Hydrogen Electrocatalysis in TaS_2 Nanosheets

Hamid Ghorbani Shiraz,* Zia Ullah Khan, Daniel Péré, Xianjie Liu, Yannick Coppel, Mats Fahlman, Mikhail Vagin, Radoslaw Chmielowski, Myrtil L. Kahn, Magnus Berggren, and Xavier Crispin*

Cite This: J. Phys. Chem. C 2023, 127, 5825−5832

Read Online

ACCESS | Metrics & More | Article Recommendations | Supporting Information

ABSTRACT: Sustainable production of hydrogen gas, a green energy carrier of high density, is possible only by electrolysis of water based on the hydrogen evolution reaction (HER). Here, we report the effect of oxygen poisoning on the efficiency of hydrogen production and the consumption by the HER and the hydrogen oxidation reaction (HOR), respectively, on the interface of platinum group metal-free electrocatalyst TaS_2 in pristine form and intercalated by the organic Lewis base hexylamine. The state of the surface probed by photoelectron spectroscopy was significantly altered by both Lewis base doping and oxygen poisoning. This alteration dramatically affects the hydrogen production efficiency in the HER, while the back process by the HOR was less sensitive to the changes in the surface states of the electrocatalysts. The oxygenated and intercalated electrocatalyst shows more than 2×10^5 times lower exchange current density of the HER compared to pristine oxygenated materials.

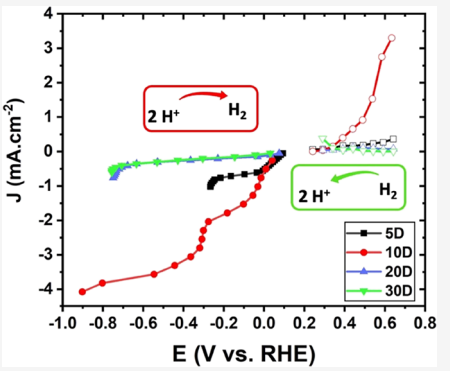

INTRODUCTION

Sustainable technologies of hydrogen production mainly rely on water electrolysis using electrical energy accessible from renewable sources. One of the losses in the conversion of applied electrical energy into hydrogen gas is due to the slow kinetics of the hydrogen evolution reaction (HER) and the auxiliary reaction of oxygen evolution. To decrease the losses, specific electrocatalysts must be designed for those reactions. The price of the electrocatalysts is one of the prime factors limiting the commercialization of sustainable hydrogen production. This motivates our effort in researching new electrocatalysts free from noble platinum group metals.

Transition metal disulfides (TMDs) have demonstrated a significant activity for the HER.[1,2] Yu et al. studied an array of TaS_2 with fantastic functionality for the HER. Ta−TaS_2 delivers a high current density of 2000 mA cm^{-2} at a relatively low overpotential of 398 mV, benefiting from near-zero contact resistance and a high degree of mechanical robustness.[3] The type of crystalline structure for TaS_2 has significant effects on the overpotential of the catalyst for the HER. The activity of 2H-TaS_2 and 1T-TaS_2 phases showed poor HER activity, but good ORR activity,[4] while the 3R phase displayed outstanding performance for the HER.[5] An overall strategy to design an electrocatalytic layer is to introduce nanoscale structures which promote a high rate for the HER and the hydrogen oxidation reaction (HOR) through the presence of a large interface area between the electrolyte and the catalyst available for the electron transfer and the molecular sorption. In that context, TaS_2 nanostructures show considerable activity toward the HER and HOR.[2] Recently, it was revealed that surface-distributed oxygen groups could be a part of the active sites for the HER[6,7] acting as proton acceptors yielding a fast electron transfer and/or an increase of the electrochemically available surface area.[8,9]

Functionalization of TMDs with organic intercalants in the van der Waals gaps of the two-dimensional (2D) materials offers a new degree of freedom to design electrocatalysts. For instance, there are many reports on metal oxides, which are decorated with alkylamines.[10] Among them, functional photocatalytic metal oxide nanoparticles with alkylamines terminate[11] or nanocrystals for perovskite applications[12] and reusable catalysts[13] could be mentioned. However, the nanostructures of TMDs functionalized with alkylamines have also displayed an opportunity to fully passivate the electrocatalyst.[13] Hence, the promotion of the HER by functional organic intercalants cannot take place in a fully intercalated system but would require partially intercalated systems as well as new functional groups of the organic intercalant to promote electronic or protonic transport in the interlayer gaps. However before considering those more advanced cases, it is crucial to understand the stability of the

Received: February 6, 2023
Revised: March 7, 2023
Published: March 17, 2023

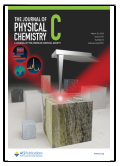

bonds between the organic intercalant and the TMDs and the effect of O_2 oxidation.

Recently, different strategies have been undertaken to manipulate the stability and control of the oxidation level of 2D inorganic nanostructures. X-ray photoelectron spectroscopy (XPS) measurements of the MoS_2 and WS_2, intercalated using alkylamines, were performed in an organic solvent. It was found that the S2p core level XPS spectrum reveals the presence of an oxygen atom attached to the sulfur.[14] In our previous study, we confirm the formation of S−O bonds together with the formation of Ta−O bonds in our 3R-TaS_2 nanosheets.[2] The origin of it is not fully clarified, but the adsorption of atmospheric water and dioxygen is a key ingredient to trigger the redox oxidation of the TMDs (e.g., through corrosion). The following absorptions are expected to be impacted by the hydrophobicity of the alkylamine that is related to the length of the alkyl group. The study mentioned above indicates that the intensity of the XPS signal related to the sulfur bonded to oxygen is inversely correlated with the amine chain length, which was proposed to be due to the reactivity of amines.[14]

Related to those findings, another 2D material is black phosphor that has been functionalized with alkylamine. Here, XPS reveals the presence of P−O bonds, also suggesting partial oxidation of the surface of the nanosheet but also the stabilization of the optoelectronic properties of black phosphor by the alkylamine.[15] Bare black phosphor is quickly oxidized from the dissolved oxygen in liquid hexylamine, leading to the formation of P−OH on the surface. These hydroxyl groups (acidic) undergo proton exchange with the NH_2 in hexylamine (as a base), the so-called Brønsted−Lowry reaction. This would form a passivation layer of hexylamine developed on the surface.[15] The stability of the alkylamine functionalized 2D sheet of black phosphor is associated with the hydrophobic role of hexylamine which acts as an agent that removes water molecules, consequently, forming a dry layer of black phosphor stable in air.

Hence, it appears that the sorption of alkylamine on 2D materials like TMDs or black phosphors is accompanied by some level of protection for the oxidation from residual impurities such as dissolved O_2 but also some level of deactivation of the catalytic properties. The interplay between the two effects has not been studied. We also need to mention the fact that the further oxidation of TMDs could result in some surface fraction of metal oxide. The alkylamine attached to the metal sulfide could lead to species such as metal oxide interacting with alkylamine. There exists a true dynamic of the alkylamine chemisorbed on the surface of metal oxide. It has been shown for instance that primary alkylamines chemisorbed on ZnO are rather immobile while secondary alkylamine can diffuse on the surface.[16] The systematic oxidation of intercalated TMDs in air has been poorly studied, even less the impact of the oxidation on their properties.

In our last study, we report the fantastic performance of 3R-TaS_2 toward the HER and HOR.[2] In connection with the last report, the study of functionalization of the efficient 3R-TaS_2 would enlighten a pathway toward the durability and oxygen compatibility of the electrode. Herein, we study the effect of oxygen-containing groups at the TaS_2 surface on bidirectional hydrogen electrocatalysis. Both the treatment with an organic Lewis base and exposure to the oxygen of air were evaluated by photoelectron spectroscopy and electrochemical techniques. The efficiency of the HER showed high sensitivity to oxygen exposure while the HOR as the backward process was less sensitive to alteration of the surface states.

METHODS

Electrochemical Characterization. Both pristine and intercalated samples of TaS_2 were kept in a common atmosphere environment for 5, 10, 20, and 30 days (named 5D, 10D, 20D, and 30D, respectively). All other chemicals were used as received.

Electrochemical measurements were carried out using a BioLogic SP200 potentiostat and a three-electrode setup in hydrogen-saturated 0.5 M H_2SO_4 solution with an IR-drop correction. A hydrophilized graphite felt was used as a counter electrode to achieve a high surface area while avoiding any platinum contamination.[17] Ag/AgCl and a rotating disk electrode (RDE, at a rotation of 800 rpm) made from glassy carbon are used as reference and working electrodes, respectively. The measurements were limited to the negative current density of 10 mA cm^{-2} to avoid peeling off the catalyst layer from the RDE. All the potentials are converted to a reversible hydrogen electrode using the Nernst equation; in 0.5 M H_2SO_4 (pH = 0), the equation is simplified as

$$E(\mathrm{RHE}) = E(\mathrm{SCE}) + 0.242\ \mathrm{V}.$$

Material Synthesis and Ink Formulation. A solution of 5 wt % Nafion (in a mixture of water and ethanol) was used as a proton-conductive binder. This solution was used to prepare 0.05 g L^{-1} mixture out of the pristine powder of TaS_2. Tantalum (Ta) and sulfur (S) powders were purchased from Goodfellow while hexylamine (HA) $C_6H_{15}N$ was bought from Sigma-Aldrich and used as received. A stoichiometric mixture of Ta and S in an agate mortar was transferred to a quartz ampoule. The ampoule was heated at 900 °C for 48 h in a furnace. Next, it was cooled down to room temperature. In the N_2 atmosphere, the as-prepared sample was postheated at 650 °C to produce the pristine sample. The intercalation of the pristine sample was carried out by HA treatment in a mixture molar ratio of 20:1 in an N_2 atmosphere, while it was stirred at 50 °C for 5 days.

Surface Characterization. XPS/UPS (X-ray, ultraviolet photoemission spectroscopy) measurements have been performed in a Scienta ESCA 200 system under a base pressure of 2E-10 mbar with a SES 200 electron analyzer, a monochromatic Al K_α X-ray source ($h\nu$ = 1486.6 eV), and a helium discharge lamp ($h\nu$ = 21.22 eV) for XPS and UPS, respectively. All spectra were collected at normal emission and room temperature. The spectrometer was calibrated by a sputter-cleaned Au film with the Fermi level at 0 eV and Au $4f_{7/2}$ peak at 84.0 eV with its full width at half maximum (FWHM) being 0.65 eV for XPS. The total energy resolution of UPS is about 0.08 eV estimated from the width of the Fermi edge of a clean Au film. The work function of the sample was extracted from the edge of the secondary electron cutoff in the UPS spectrum with a bias of −3 V applied in the sample.

Nuclear magnetic resonance (NMR) experiments were recorded on a Bruker Avance 400 III HD spectrometer operating at magnetic fields of 9.4 T. Samples were packed into 2.5 mm zirconia rotors under argon inside a glove box. The rotors were spun between 10 and 15 kHz at 295 K. ^{1}H MAS was performed with the DEPTH pulse sequence and a recycle delay of 3 s. Chemical shifts were externally referenced to liquid TMS. The NMR experiments had to be realized in small

https://doi.org/10.1021/acs.jpcc.3c00825
J. Phys. Chem. C 2023, 127, 5825−5832

rotors (2.5 mm) because of the unfavorable electromagnetic properties of the samples.

RESULTS

Crystal Structure Investigation. X-ray diffraction (XRD) patterns have been collected at each step of the material synthesis (Figure 1). The XRD peaks collected from the

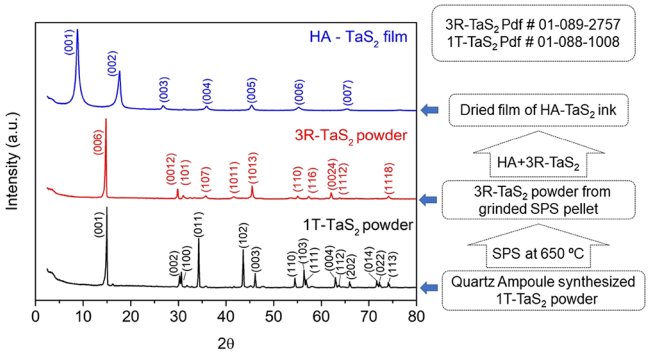

Figure 1. XRD pattern for the intermediate and products. The material that is synthesized in the ampoule shows the 1T-TaS_2; after post-treatment, the 3R-TaS_2 and hexylamine-intercalated 3R-TaS_2 (HA-TaS_2) were successfully formed.

powder after the quartz ampoule synthesis correspond to the 1T-TaS_2 (PDF # 01-088-1008) with a characteristic interplanar distance (001) of about 6.10 Å while the XRD recorded on the powder after a quick ramp at 650 °C fits with 3R-TaS_2 (PDF # 01-089-2757) and its characteristic (001) peak of about 6.03 Å. The comparison of these two diffractograms clearly indicates that a phase transition from 1T-TaS_2 to 3R-TaS_2 occurs during the spark plasma sintering step. During the next step of the synthesis, the 3R-TaS_2 powder has been mixed with hexylamine (HA). The resulting XRD corresponds to a superlattice structure characterized by a series of (00*l*). All the observed peaks can be indexed as follows: (001) at 10.06 Å, (002) at 5.01 Å, (003) at 3.32 Å, (004) at 2.50 Å, (005) at 2.00 Å, (006) at 1.66 Å, and (007) at 1.43 Å. It is worth mentioning that the peak up to (007) is clearly detected; this means that the obtained HA-TaS_2 superlattice has high crystal quality. Moreover, all the peaks observed on 1T-TaS_2 and 3R-TaS_2, including strong (001) and (006) peaks, are totally absent from the new superlattice HA-TaS_2. This indicates that the hexylamine is fully intercalated into the van der Waals planes of TaS_2, and its interplanar distance increases from about 6.03 to 10.06 Å.

Spectroscopic Investigation of Surface and Bulk. To illustrate the influence of the intercalation with HA on the electronic properties of TaS_2, X-ray and ultraviolet photoelectron spectroscopy (XPS/UPS) methods have been used. The XPS Ta 4f peak of the pristine TaS_2 indicated that there are two different types of Ta valency (left panel in Figure 2A). The Ta 4f doublet between 22 and 25 eV is from the pristine TaS_2, while the doublet between 25 and 30 eV is attributed to the surface oxidation of TaS_2[18,2] due to exposure to air. Upon HA treatment, the doublet from the oxide is significantly decreased or shifted into the low binding energy doublet. This suggests that the alkylamine gives part of its electronic density (electron donor character) to TaS_2 and its fraction of surface oxide thus moving them toward low binding energy. This is typical of a dative coordination mode of HA to the Ta through

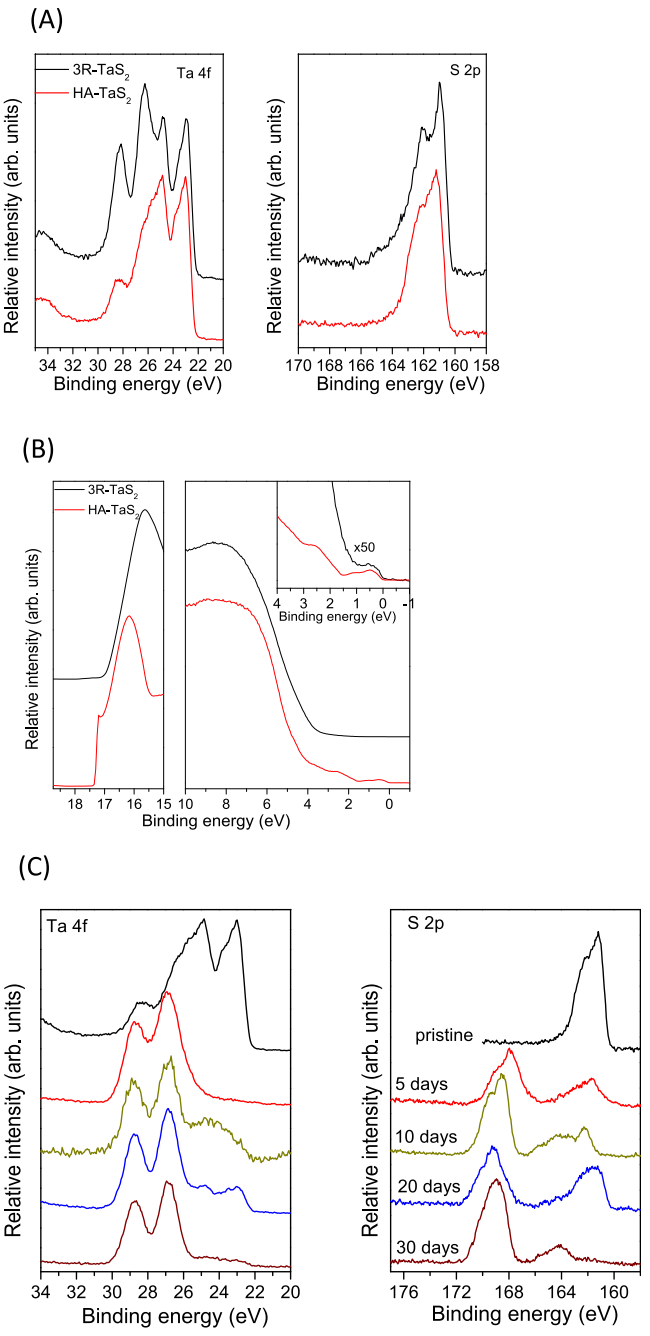

Figure 2. XPS data for samples. The oxygen contamination is recognized in all measurements; (a) Ta 4f peak shows two different types of Ta in examined samples (pristine and HA-treated), and similar spectral features of S2p; (b) UPS spectra and inset of valence feature close to the Fermi level for both pristine and HA-treated samples; (c) comparative Ta 4f and S2p spectra for all samples.

the free doublet of the amine nitrogen atom.[19] Correspondingly, the spectral feature of S2p (right panel in Figure 2A) from the pristine and HA-intercalated TaS_2 shows a very similar character, with only a slight decrease in spectral intensity at the higher binding energy (ca. 164 eV) and shifting to the higher binding energy (ca. 0.15 eV) after HA treatment. This confirms that the coordination of HA is on the Ta atoms rather than the S atoms. All the XPS data indicate that there is a strong interaction between TaS_2 and HA, and the obvious change of the electronic properties after HA treatment is

https://doi.org/10.1021/acs.jpcc.3c00825
J. Phys. Chem. C 2023, 127, 5825−5832

directly coupled to the HA intercalation in the van der Waals gaps of the layered TaS_2 as demonstrated by XRD results.

Furthermore, upon HA intercalation, the secondary electron cutoff of the UPS spectra (left panel in Figure 2B) demonstrated a 0.4 eV decrease of the work function (from 4.3 to 3.9 eV for pristine and intercalated TaS_2, respectively), which is in line with the XPS data indicating a bond formation between the Ta atoms and the HA. The lower work function after doping could indicate the formation of a surface dipole resulting from the electron density displaced from the electron doublet of the nitrogen toward the orbitals of the Ta atoms. The non-intercalated TaS_2 displays a weak density of state at the Fermi level attributed to the 5d band.[20] The most significant change of the UPS spectra upon HA intercalation is the appearance of three valence electronic levels at 0.5, 1, and 1.5 eV from the Fermi level (inset of the right panel in Figure 2B), where there is almost no visible feature in the pristine TaS_2 but becomes very strong after HA treatment (right panel in Figure 2B). It can be seen that the valence band feature can be enhanced around 50 times in the intercalated TaS_2 compared to the pristine one.

We now turn to the oxidation of the HA-intercalated TaS_2 in air versus time. Upon air exposure, the HA-intercalated TaS_2 showed oxidation signs visible in the evolution of XPS by an enhanced O1s peak, but also a significant modification of the Ta4f and S2p spectra versus air exposure time (Figure 2C). The low binding energy doublet in the Ta4f spectrum was strongly suppressed; meanwhile, the doublet at high energy (27 and 29 eV) is significantly enhanced. In the literature, the thermally oxidized 2D layer of TaS_2 can be transformed into Ta_2O_5 as identified by the Ta4f of the doublet at 26 and 28 eV.[21] The situation of the spontaneously oxidized HA-intercalated TaS_2 is certainly not giving the pure Ta_2O_5 but rather another complex composition with sulfur oxide groups (possibly with SO_2 groups as proposed in the theoretical study[22]) since the Ta4f doublet is shifted by 1 eV toward high energy. After 30 days of exposure, the Ta4f feature from intercalated TaS_2 is close to almost completely suppressed; instead, the oxidized Ta is dominant because of the oxidation of intercalated TaS_2 in air. When we turn to the XPS S2p peak of intercalated TaS_2, a new feature at high binding energy (between 168 and 172 eV) appears upon air exposure, while the original S2p feature (between 160 and 164 eV) becomes very weak. The new contribution at high binding energy indicates that the sulfur gets bonded to an electronegative atom supposedly oxygen as found on the surface of other metal sulfides.[14] Theoretical modeling of the first step of the oxidation of 2H-TaS_2 indicates a preference for the oxygen atoms to be absorbed on the edge of the nanosheets at the bridge position between edge S and Ta atoms. Hence, the oxygen is in direct contact with both the Ta and the S atoms through new covalent bonds.[22] Another theoretical study supports that 1T-TaS_2 is oxidized at their edges upon exposure to oxygen/air.[23] Note that the valence band feature of intercalated TaS_2 in UPS (Figure 2B) was completely suppressed after 5 days of air exposure indicating the opening of the band gap since the formed tantalum oxide or tantalum sulfur oxide is an insulator and that explains the decrease in conductivity. Note also that the work function of the HA-intercalated TaS_2 is only slightly increased with air exposure, which may point out that there will be no significant change in the barrier of the charge transfer in the HER electrochemical reaction.

^{1}H MAS NMR experiments were performed on pristine Ta_2S and HA-functionalized Ta_2S before and after 72 h of air exposure. The technique probes the bulk of the sample instead of the top surface investigated by XPS/UPS. The pristine Ta_2S ^{1}H MAS spectrum exhibits one broad peak centered at 3 ppm characteristic of hydroxide groups of surfaces OH or/and isolated physisorbed water molecules (Figure 3A). This signal

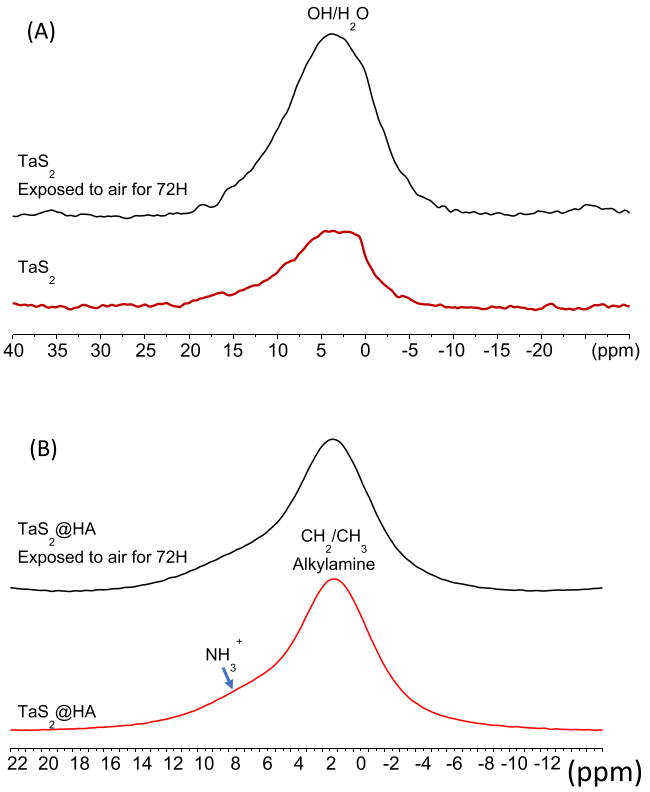

Figure 3. (a) ^{1}H MAS spectrum of pristine TaS_2 before and after 72 h of air exposure. (b) ^{1}H MAS spectrum of HA-intercalated TaS_2 before and after 72 h of air exposure.

shifts to 3.9 ppm with an intensity increase after air exposure indicating an increase in the number of OH groups on the surface and/or in the number of water molecules absorbed. For HA-functionalized TaS_2, the ^{1}H MAS spectra (Figure 3B) show, in addition to the characteristic alkylamine peak at 3 ppm, a shoulder at 7 ppm attributable to ammonium. Exposure of the HA-functionalized sample to air did not change the shape of the signals, suggesting that there was no evolution of the material. The presence of amines, therefore, plays, as expected, an important role in protecting the material from oxidation effects.

HER/HOR Electrocatalysis. The catalytic layer that is coating the glassy carbon electrode for electrochemical characterization is composed of the TaS_2 catalyst particles for the HER and the Nafion ionomer binder that promotes the transport of protons. The TaS_2 particles are electrically conducting and form a percolation path for the electronic transport. Morphology investigation of the catalytic layer (Figure 4) showed a nanocomposite made of catalyst nanoflakes embedded in a Nafion fluoropolymer matrix. We also characterized the samples using energy-dispersive X-ray (EDX) analysis and detected everywhere the presence of Nafion (points 1, 2, and 3 display a F signal), but there is also

https://doi.org/10.1021/acs.jpcc.3c00825
J. Phys. Chem. C 2023, 127, 5825−5832

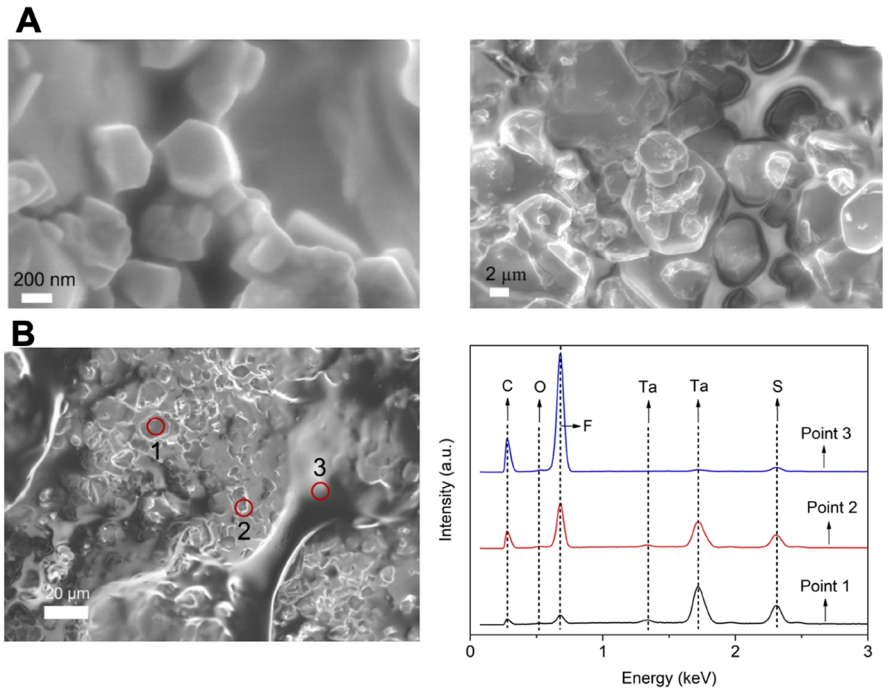

Figure 4. Microstructure measurements. (a) SEM images of the catalytic layer (at 5 kV); (b) EDX measurements (the SEM image is recorded at 10 kV). EDX was done at three points. Point 1 has a visible TaS_2 flake, point 2 has a TaS_2 flake and polymer next to it while point 3 shows a polymer layer hiding a TaS2 particle.

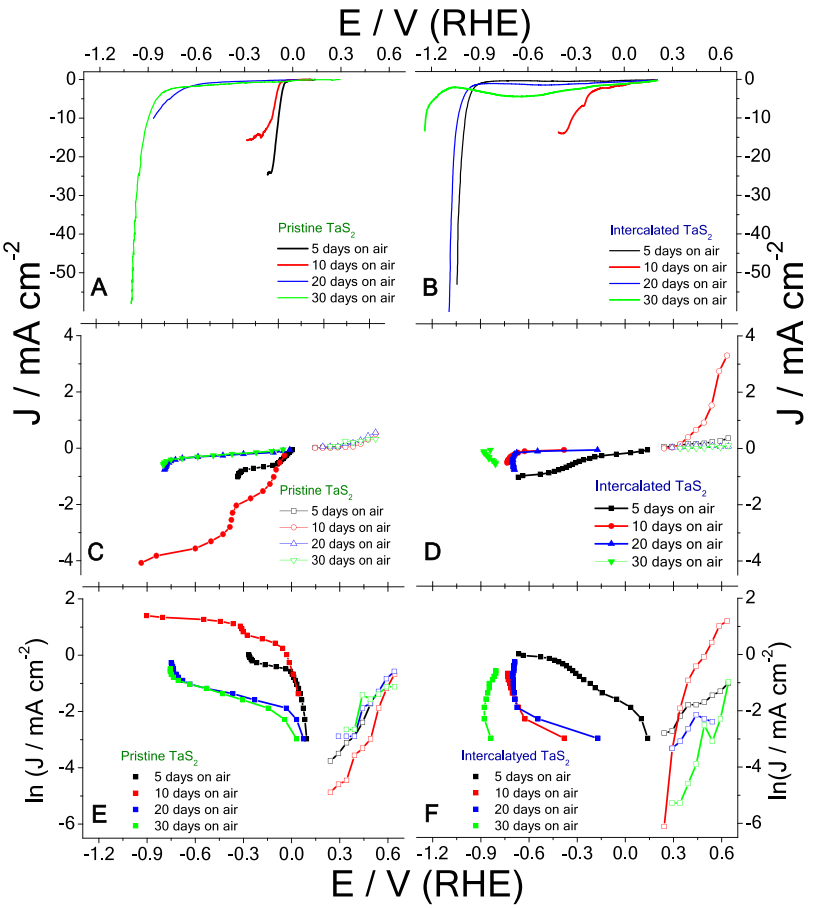

Figure 5. Oxygen poisoning on bidirectional HER/HOR electrocatalysis. The pristine (A,C,E) and intercalated (B,D,F) TaS_2-modified RDE subjected to linear sweep voltammetry (A,B) and *iR*-corrected steady-state voltammetry (in linear (C,D) and Tafel (E,F) coordinates; oxidation and reduction currents are presented as open and filled symbols); hydrogen-saturated 0.5 M H_2SO_4.

https://doi.org/10.1021/acs.jpcc.3c00825
J. Phys. Chem. C 2023, 127, 5825−5832

some area rich in TaS_2 (e.g., point 1) or in Nafion (e.g., point 3).

Linear sweep voltammetry performed in the acidic oxygen-free environment on a glassy carbon electrode modified with the catalytic layers using either pristine 3R-TaS_2 particles or HA-intercalated TaS_2 particles illustrates an HER activity. The applied voltage ramp in the negative direction yields the appearance of high negative currents (Figure 5A,B) due to the HER on both electrocatalysts. The use of steady-state voltammetry (Figure 5C−F) enabled the observation of positive currents at the positive potentials applied on the electrodes related to the HOR. The zero-voltage defines the thermodynamically energy threshold (reversible potential) of the faradaic reaction:

$$2H^+ + 2e^- \leftrightarrow (H_2)_{gas} \quad (1)$$

The passage of the reaction 1 from left to right illustrates the HER, while the passage in opposite direction manifests the backward process, namely, HOR. The zero-voltage located in between the potentials of HER and HOR demarcates the potentials of HER and HOR and manifests the reversible hydrogen electrode (RHE). Following the Butler−Volmer kinetics, the voltage difference applied with respect to the RHE is the driving force for the exponential faradaic currents: negative or positive currents for the HER or HOR, respectively. The logarithm scale of the current versus voltage yields the Tafel plots (Figure 5E,F). Importantly, the fast proton transport by the Grotthuss mechanism[24] ensures the absence of the mass transport limitations of HER currents. HER currents are independent of rotation; therefore, they are diffusion-free. This implies that the kinetics of the heterogeneous electron transfer in the reaction 1 defines the observed HER currents.

Consistent with our previous report, the HA-intercalated TaS_2 showed a significant decrease in the observed HER currents in comparison with the pristine sample; thus HA intercalation manifests an electrocatalyst poisoning effect.[2] The HA-intercalated TaS_2 electrode required substantially larger negative voltage, so-called overpotential (Figure 5B), in comparison with the pristine 3R-TaS_2 electrocatalyst (Figure 5A). The exposure of the catalyst to air modifies the HER activity due to a surface oxidation process as displayed by XPS (Figure 2C).

However, there is a complex behavior of the HER/HOR activities versus the air exposure time. Indeed, the HER on pristine and HOR on intercalated TaS_2 showed maximum activity after 10 days of exposure. The electrocatalytic activity toward the HER is also more sensitive to air exposure in comparison with the HOR. In the contrast to pristine TaS_2, the HA-intercalated TaS_2 showed a dramatic decrease in the rate of the HER with prolonged exposure to air. Indeed, the extrapolation of kinetic currents of the same rate-determining step of the HER manifested with the equal values of Tafel slope on the zero overpotential enabled the estimation of exchange current densities (Figure 6A). The HER on pristine and intercalated TaS_2 exposed to air for 10 days showed values of exchange current densities of 0.061 mA cm^{-2} and 2.9×10^{-7} mA cm^{-2} representing the dramatic effect of oxygen poisoning on the state of the electrocatalyst surface. Both pristine and intercalated electrocatalysts showed nonmonotonous steady-state polarization curves for the HER (Figure 5E,F). Excluding the fast reactant (proton) transport, this might illustrate the

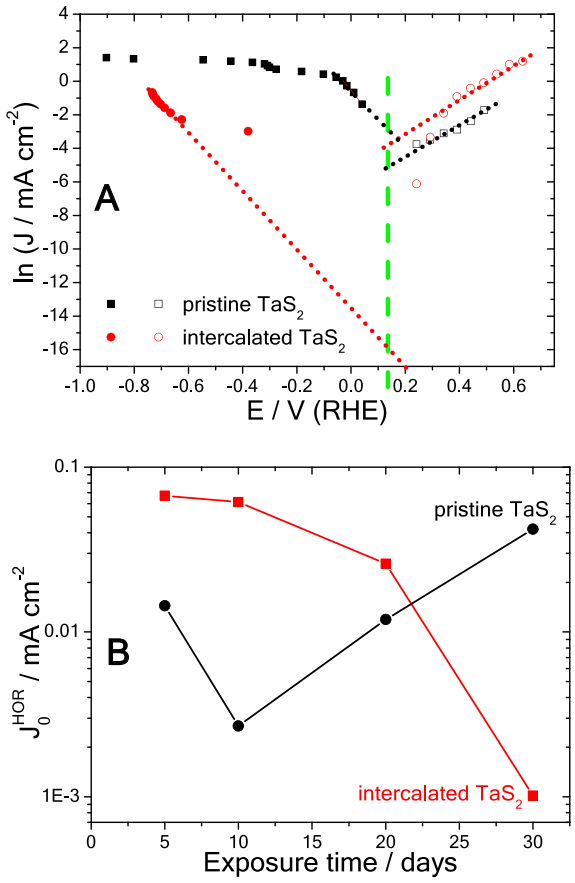

Figure 6. Effect of oxygen poisoning on HOR and HER kinetics on pristine and intercalated TaS2. (a) *iR*-corrected steady-state voltammograms obtained on GCE modified with pristine and intercalated TaS_2 after 10 days of air exposure (black and red symbols, respectively) in Tafel coordinates (oxidation and reduction currents are presented as open and filled symbols, respectively; hydrogen-saturated 0.5 M H_2SO_4); (b) dependence of HOR exchange current densities on pristine and intercalated TaS_2-modified GCEs (black and red symbols, respectively) on the air exposure time.

limitation of the slow product (hydrogen) mass transport on the electrocatalyst.

The HOR currents on pristine electrocatalysts showed insensitivity to oxidation by air exposure with the confinement of the Tafel slope of ca. 120 mV dec^{-1}, which is frequently reported for a variety of HOR electrocatalysts.[25] The extrapolation of the linear region of air-insensitive HOR currents allowed the estimation of the HOR exchange current density as a driving force-free rate of the process. In contrast to pristine TaS_2, the intercalated electrocatalyst showed a significant decrease of HOR exchange current upon prolonged exposure to air (Figure 6B). The exchange current densities for the HOR estimated for pristine TaS_2 are comparable with the values obtained on gold (0.027 mA cm^{-2}) and significantly smaller than on platinum (0.78 mA cm^{-2}).[2]

The normalization of observed HER/HOR current densities by the total mass of catalyst-based slurry deposited onto the electrode (Figure S1A,B) was utilized for the estimation of the oxygen poisoning effect on the mass activity of electrocatalysts.[26] Coherently, the capacitive current densities recorded by voltammetry at the potentials far from the potentials of any faradaic processes (e.g., at 0.2 V (vs RHE) in the nitrogen-saturated electrolyte) represent the electrochemi-

https://doi.org/10.1021/acs.jpcc.3c00825
J. Phys. Chem. C 2023, 127, 5825−5832

cally available surface area (EASA) of investigated electrocatalytic interfaces. The normalization of observed HER/HOR currents by the EASA-representing capacitive currents (Figure S1C–D) was used for the estimation of the oxygen poisoning effect on the surface activity of the electrocatalysts.[26] Importantly, both mass- and EASA-normalized HER/HOR currents showed similar trends on steady-state voltammograms with the increase of exposure time on air validating the oxygen poisoning effect visible by raw current densities.

DISCUSSION

The NMR data indicate that the alkylamine molecules are still present in the bulk of the van der Waals gaps of the TaS_2 after exposure to air and that this slows down the bulk oxidation or creation of hydroxide. The XPS investigation reveals a strong surface oxidation of the HA-intercalated TaS_2. The appearance of the SO_x spectral feature in the S2p in the HA-intercalated TaS_2 upon air exposure agrees with what is theoretically predicted for the early oxidation step of the non-intercalated TaS_2. This indicates the presence of oxygen atoms in the bridge between the Ta and S atoms; thus, new Ta–O bonds and S–O bonds are in agreement with the Ta4f and S2p spectra. Hence, a question arises: what happens to the alkylamine attached to the Ta atoms upon air exposure?

The HER current can be seen as a probe to reveal the surface state of the TaS_2 since its 3R-form is a good catalyst with almost no overpotential. The intercalation with HA completely passivates the catalytic effect since HA attaches to the Ta surface atoms through donating coordination between the lone pair of the nitrogen and the d-orbitals of Ta. Another type of bond is formed through an acid–base reaction between the Ta–OH surface groups and the NH_3-hexyl, leading to an $(NH_4)^+$-hexyl. The presence of the ammonium is supported by the NMR data (the shoulder at +7 ppm in Figure 3B). The non-intercalated TaS_2 displays a drop in the HER current due to the formation of a surface oxide that passivates the catalytic sites. The air exposure of the HA-intercalated TaS_2 leads to a surprising behavior since it goes from a passivated catalysis due to the HA chemisorption, to a clear catalytic activity for the HER after a certain time of exposure to air (10 days). We hypothesize that there is a removal of the alkylamine from the Ta catalytic sites upon the oxidation accompanied by the location of oxygen atoms in the bridge position between Ta and S (new Ta–O and S–O bonds). The catalytic sites formed upon alkylamine removal upon oxidation are most likely not similar to the catalytic sites present on the pristine non-intercalated TaS_2. Indeed, the HOR current obtained is much larger with the partially oxidized HA-intercalated TaS_2 (10 days) than the pristine TaS_2 (Figure 5C vs D). Note that after longer exposure to air (>10 days), the catalytic activity for the HER and HOR collapses, and we attribute that to the dominating oxidation of TaS_2 through the surface removal of HA, similar to found for non-intercalated TaS_2.

Note that the electrocatalytic activity toward the HER is also more sensitive to air exposure in comparison with the HOR. Some other factors could potentially play a role. The proceeding of HER (reaction 1 from left to right) involves the formation of a new phase, namely, hydrogen gas. Following the theory of the critical bubble formation, the surface tension between the electrolyte solution and the electrochemical interface affects the rate of the electrode reaction, which involves the product or reagent in a form of a new phase such as gas (e.g., HER) or solid (e.g., electrodeposition).[27] In contrast, the HOR involves hydrogen in a dissolved form, which implies insensitivity to surface tension.

CONCLUSIONS

Our study reveals the importance of oxygen species on the catalytic effects of TaS_2. A good catalytic activity for the HER is found for the non-intercalated TaS_2 containing some level of oxygen species on its surface, a fact also found in other studies. While the HA-intercalated TaS_2 significantly blocks the catalytic activity of HER, a short-time exposure to air recovers some level of HER activity. This suggests the removal of the alkylamine on the Ta atoms as well as the involvement of surface oxygen species in the catalytic site for the HER. The oxidation of the HA-intercalated TaS_2 reveals a state of oxidation where new catalytic sites are formed with a remarkably high current for the HOR. Hence, both doping by Lewis acid and exposure to oxygen showed a significant effect on the efficiency of HER/HOR electrocatalysis on TaS_2. For long exposure times, the TaS_2 is likely devoid of alkylamine and is further oxidized, and like the non-intercalated TaS_2, the metal sulfur oxide passivates the catalytic sites. Importantly, the bulk of the samples seems unaffected by the surface oxidation as the hexylamine is invariably present in the van der Waals gaps.

ASSOCIATED CONTENT

Supporting Information

The Supporting Information is available free of charge at https://pubs.acs.org/doi/10.1021/acs.jpcc.3c00825.

Normalized Tafel plots for the HER and HOR (PDF)

AUTHOR INFORMATION

Corresponding Authors

Hamid Ghorbani Shiraz – *Laboratory of Organic Electronics, Department of Science and Technology, Linköping University, Norrköping 60174, Sweden;* orcid.org/0000-0002-2001-1538; Email: Hamid.ghorbani.shiraz@liu.se

Xavier Crispin – *Laboratory of Organic Electronics, Department of Science and Technology and Wallenberg Wood Science Center, Department of Science and Technology, Linköping University, Norrköping 60174, Sweden;* orcid.org/0000-0001-8845-6296; Email: Xavier.crispin@liu.se

Authors

Zia Ullah Khan – *Laboratory of Organic Electronics, Department of Science and Technology, Linköping University, Norrköping 60174, Sweden*

Daniel Péré – *Department of Advanced Materials, IMRA Europe S.A.S., Sophia Antipolis 06904, France*

Xianjie Liu – *Laboratory of Organic Electronics, Department of Science and Technology, Linköping University, Norrköping 60174, Sweden;* orcid.org/0000-0002-3190-2774

Yannick Coppel – *LCC-CNRS, University of Toulouse, CNRS, Toulouse 31077, France;* orcid.org/0000-0003-0970-4082

Mats Fahlman – *Laboratory of Organic Electronics, Department of Science and Technology, Linköping University, Norrköping 60174, Sweden;* orcid.org/0000-0001-9879-3915

https://doi.org/10.1021/acs.jpcc.3c00825
J. Phys. Chem. C 2023, 127, 5825–5832

Mikhail Vagin − *Laboratory of Organic Electronics, Department of Science and Technology, Linköping University, Norrköping 60174, Sweden*

Radoslaw Chmielowski − *Department of Advanced Materials, IMRA Europe S.A.S., Sophia Antipolis 06904, France*

Myrtil L. Kahn − *LCC-CNRS, University of Toulouse, CNRS, Toulouse 31077, France;* orcid.org/0000-0003-3079-5759

Magnus Berggren − *Laboratory of Organic Electronics, Department of Science and Technology and Wallenberg Wood Science Center, Department of Science and Technology, Linköping University, Norrköping 60174, Sweden;* orcid.org/0000-0001-5154-0291

Complete contact information is available at: https://pubs.acs.org/10.1021/acs.jpcc.3c00825

Notes

The authors declare no competing financial interest.

■ ACKNOWLEDGMENTS

This work was financially supported by the Swedish Research Council (VR 2016-05990 and VR 2020-04210), the Knut and Alice Wallenberg Foundation (KAW 2019.0604; 2021.0195), Karl Erik Önnesjös Foundation, and the Swedish Government Strategic Research Area in Materials Science on Advanced Functional Materials at Linköping University (Faculty Grant SFO-Mat-LiU No. 2009-00971).

■ REFERENCES

(1) Bonde, J.; Moses, P. G.; Jaramillo, T. F.; Nørskov, J. K.; Chorkendorff, I. Hydrogen Evolution on Nano-Particulate Transition Metal Sulfides. *Faraday Discuss.* **2009**, *140*, 219−231.

(2) Ghorbani Shiraz, H.; Ullah Khan, Z.; Péré, D.; Liu, X.; Coppel, Y.; Fahlman, M.; Berggren, M.; Chmielowski, R.; Kahn, M. L.; Vagin, M.; Crispin, X. 3R-TaS_2 as an Intercalation-Dependent Electrified Interface for Hydrogen Reduction and Oxidation Reactions. *J. Phys. Chem. C* **2022**, *126*, 17056−17065.

(3) Yu, Q.; Zhang, Z.; Qiu, S.; Luo, Y.; Liu, Z.; Yang, F.; Liu, H.; Ge, S.; Zou, X.; Ding, B. A Ta-TaS_2 Monolith Catalyst with Robust and Metallic Interface for Superior Hydrogen Evolution. *Nat. Commun.* **2021**, *12*, 6051.

(4) Luxa, J.; Mazánek, V.; Pumera, M.; Lazar, P.; Sedmidubský, D.; Callisti, M.; Polcar, T.; Sofer, Z. 2H → 1T Phase Engineering of Layered Tantalum Disulfides in Electrocatalysis: Oxygen Reduction Reaction. *Chem. −Eur. J.* **2017**, *23*, 8082−8091.

(5) Feng, Y.; Gong, S.; Du, E.; Chen, X.; Qi, R.; Yu, K.; Zhu, Z. 3R TaS_2 Surpasses the Corresponding 1T and 2H Phases for the Hydrogen Evolution Reaction. *J. Phys. Chem. C* **2018**, *122*, 2382−2390.

(6) Ifires, M.; Addad, A.; Barras, A.; Hadjersi, T.; Chegroune, R.; Szunerits, S.; Boukherroub, R.; Amin, M. A. Cathodic Pre-Polarization Studies on the Carbon felt/KOH Interface: An Efficient Metal-Free Electrocatalyst for Hydrogen Generation. *Electrochim. Acta* **2021**, *375*, No. 137981.

(7) Ding, J.; Sun, X.; Wang, Q.; Li, D.-S.; Li, X.; Li, X.; Chen, L.; Zhang, X.; Tian, X.; Ostrikov, K. K. Plasma Synthesis of Pt/G-C_3N_4 Photocatalysts with Enhanced Photocatalytic Hydrogen Generation. *J. Alloys Compd.* **2021**, *873*, No. 159871.

(8) Tan, S. M.; Ambrosi, A.; Chua, C. K.; Pumera, M. Electron Transfer Properties of Chemically Reduced Graphene Materials with Different Oxygen Contents. *J. Mater. Chem. A* **2014**, *2*, 10668−10675.

(9) Huang, Y.; Sun, L.; Yu, Z.; Jiang, R.; Huang, J.; Hou, Y.; Yang, F.; Zhang, B.; Zhang, R.; Zhang, Y. Adjustable Anchoring of Ni/Co Cations by Oxygen-Containing Functional Groups on Functionalized Graphite Paper and Accelerated Mass/Electron Transfer for Overall Water Splitting. *Catal. Sci. Technol.* **2020**, *10*, 2627−2643.

(10) Kahn, M. L.; Glaria, A.; Pages, C.; Monge, M.; Saint Macary, L.; Maisonnat, A.; Chaudret, B. Organometallic Chemistry: An Alternative Approach Towards Metal Oxide Nanoparticles. *J. Mater. Chem.* **2009**, *19*, 4044−4060.

(11) Borah, R.; Ninakanti, R.; Nuyts, G.; Peeters, H.; Pedrazo-Tardajos, A.; Nuti, S.; Vande Velde, C.; De Wael, K.; Lenaerts, S.; Bals, S. Selectivity in the Ligand Functionalization of Photocatalytic Metal Oxide Nanoparticles for Phase Transfer and Self-Assembly Applications. *Chem. −Eur. J.* **2021**, *27*, 9011−9021.

(12) McGrath, F.; Ghorpade, U. V.; Ryan, K. M. Synthesis and Dimensional Control of $CsPbBr_3$ Perovskite Nanocrystals Using Phosphorous Based Ligands. *J. Chem. Phys.* **2020**, *152*, 174702.

(13) Hahn, G.; Kunnas, P.; de Jonge, N.; Kempe, R. General Synthesis of Primary Amines Via Reductive Amination Employing a Reusable Nickel Catalyst. *Nat. Catal.* **2019**, *2*, 71−77.

(14) Jeffery, A. A.; Nethravathi, C.; Rajamathi, M. Scalable Large Nanosheets of Transition Metal Disulphides through Exfoliation of Amine Intercalated MS_2 [M = Mo, W] in Organic Solvents. *RSC Adv.* **2015**, *5*, 51176−51182.

(15) Su, C.; Yin, Z.; Yan, Q.-B.; Wang, Z.; Lin, H.; Sun, L.; Xu, W.; Yamada, T.; Ji, X.; Zettsu, N.; Teshima, K.; Warner, J. H.; Dincă, M.; Hu, J.; Dong, M.; Su, G.; Kong, J.; Li, J. Waterproof Molecular Monolayers Stabilize 2d Materials. *Proc. Natl. Acad. Sci. U. S. A.* **2019**, *116*, 20844−20849.

(16) Wang, Y.; Coppel, Y.; Lepetit, C.; Marty, J.-D.; Mingotaud, C.; Kahn, M. L. Anisotropic Growth of Zno Nanoparticles Driven by the Structure of Amine Surfactants: The Role of Surface Dynamics in Nanocrystal Growth. *Nanoscale Adv.* **2021**, *3*, 6088−6099.

(17) Gu, C.; Norris, B. C.; Fan, F.-R. F.; Bielawski, C. W.; Bard, A. J. Is Base-Inhibited Vapor Phase Polymerized PEDOT an Electrocatalyst for the Hydrogen Evolution Reaction? Exploring Substrate Effects Including Pt Contaminated Au. *ACS Catal.* **2012**, *2*, 746−750.

(18) Takeuchi, H.; Urakami, N.; Hashimoto, Y. Oxidation of Tantalum Disulfide (TaS_2) Films for Gate Dielectric and Process Design of Two-Dimensional Field-Effect Device. *Nanotechnology* **2022**, *33*, 375204.

(19) Spataro, G.; Champouret, Y.; Florian, P.; Coppel, Y.; Kahn, M. L. Multinuclear Solid-State NMR Study: A Powerful Tool for Understanding the Structure of ZnO Hybrid Nanoparticles. *Phys. Chem. Chem. Phys.* **2018**, *20*, 12413−12421.

(20) Pathan, M. A. K.; Gupta, A.; Vaida, M. E. Exploring the growth and oxidation of 2D-TaS_2 on Cu (111). *Nanotechnology* **2021**, *32*, 505605.

(21) Chamlagain, B.; Cui, Q.; Paudel, S.; Cheng, M. M.-C.; Chen, P.-Y.; Zhou, Z. Thermally Oxidized 2d TaS_2 as a High-K Gate Dielectric for MoS_2 Field-Effect Transistors. *2D Mater.* **2017**, *4*, No. 031002.

(22) Martincová, J.; Otyepka, M.; Lazar, P. Atomic-Scale Edge Morphology, Stability, and Oxidation of Single-Layer 2H-TaS_2. *ChemPlusChem* **2020**, *85*, 2557−2564.

(23) Martincová, J.; Otyepka, M.; Lazar, P. Oxidation of Metallic Two-Dimensional Transition Metal Dichalcogenides: 1T-MoS_2 and 1T-TaS_2. *2D Mater.* **2020**, *7*, No. 045005.

(24) Agmon, N. The Grotthuss Mechanism. *Chem. Phys. Lett.* **1995**, *244*, 456−462.

(25) Shinagawa, T.; Garcia-Esparza, A. T.; Takanabe, K. Insight on Tafel Slopes from a Microkinetic Analysis of Aqueous Electrocatalysis for Energy Conversion. *Sci. Rep.* **2015**, *5*, 13801.

(26) Hansen, J. N.; Prats, H.; Toudahl, K. K.; Mørch Secher, N.; Chan, K.; Kibsgaard, J.; Chorkendorff, I. Is There Anything Better Than Pt for HER? *ACS Energy Lett.* **2021**, *6*, 1175−1180.

(27) Taqieddin, A.; Nazari, R.; Rajic, L.; Alshawabkeh, A. Physicochemical Hydrodynamics of Gas Bubbles in Two Phase Electrochemical Systems. *J. Electrochem. Soc.* **2017**, *164*, E448.